

Scalar scattering from charged black holes on the brane

Ednilton S. de Oliveira*

Faculdade de Física, Universidade Federal do Pará, 66075-110, Belém, Pará, Brazil

November 24, 2022

Abstract

The differential scattering cross section of the massless scalar field localized on the 3-brane of charged static black holes in the ADD model is analyzed. While results valid in the entire range of scattering angle can be obtained only via a numerical approach, analytical results can be obtained via the geodesic and glory approximations. The comparisons between numerical and analytical results lead to excellent agreements. The increase of the charge intensity has the consequence of increasing the width of the interference fringes in the scattering cross section. Its influence on the intensity of the scattered flux, however, depends on the dimensionality of the spacetime. Analyzes for the special cases of uncharged and extremely charged black holes are included.

1 Introduction

The study of astrophysical objects has given an enormous step forward with the recent detections of gravitational waves [1]. These realizations mark the beginning of a new epoch in science, when mankind started to look into the Universe in the perspective of gravitational waves. Also, these remarkable accomplishments brought to our knowledge the existence of binary systems of stellar-mass black holes. This can be regarded as one more evidence that such objects populate the Universe in varied systems, with masses which go from some to million or even billion solar masses [2]. In the other hand, electromagnetic radiation still gives the best possibilities of probing structures around black holes with sizes comparable to their event horizons [3, 4]. In particular, one of the black hole candidates which have called most attention of astrophysicists is Sgr A*, the black hole in the center of our galaxy, with estimated mass of $\sim 4 \times 10^6 M_{\odot}$.

The possibilities mentioned above have instigated some researches about how radiation emitted near, e.g. from the accretion disk [5], and from far sources [6] are scattered in the vicinity of black holes. When enough resolution is achieved, astrophysicists will finally observe the event horizon of these black holes as a shadow [7], which can describe not only the characteristics of the black hole, as its rotation, but also input experimental constrains to alternative theories of gravity.

Although astrophysical black holes are undoubtedly the ‘labs’ for testing the strong limit of gravity, it has also increased in the recent years the effort to observe black hole properties in labs. Such efforts can be put in two categories:

*ednilton@pq.cnpq.br

one based in acoustic analogue systems [8, 9] and the other based in brane-world scenarios [10–14]. These two approaches are now in different levels; while acoustic systems have already been used to observe some of event horizon consequences, as the stimulated Hawking radiation [15, 16] and superradiance [17], the consequences of the interaction between higher-dimensional black holes and 3-brane fields still remain in the theoretical level. The appearance of black holes in particle colliders, as the LHC, is one real possibility of studying black hole phenomenology in local experiments conditioned to one of the most fundamental problems in physics: the existence of extra dimensions.

Black holes created in particle collisions would rapidly evaporate via Hawking radiation. This fact has instigated the study of scattering properties of higher-dimensional black holes, once Hawking radiation is directly related to the greybody factors which measure the probability of the black hole absorbing scattered waves. Works have been done considering mainly the Arkani-Hamed–Dimopoulos–Dvali (ADD) scenario, in which uncharged [18–24], charged [25], and rotating [26] black holes have been analyzed. Some work about wave properties, as quasinormal modes, around black holes in the Randall-Sundrum scenario has been recently developed [27, 28].

In the present work we analyze the scattering properties of a small (static) charged black hole for the massless scalar field restricted to the 3-brane in the ADD model. We compare results for black holes with different charge intensities, including the uncharged [24] and extreme cases. In Sec. 2 we present the geometry of the analyzed system as well as the general scattering properties of the massless scalar field in this geometry. In Sec. 3 we present the analytical methods used to obtain approximated results which can be compared with the numerical ones. The numerical results obtained via the partial-wave method are presented in Sec. 4 together with their comparisons with the analytical results. We present our conclusions in Sec. 5. Here we adopt the speed of light $c = 1$.

2 Wave scattering

The spacetime of higher-dimensional non-rotating charged black holes was found by Myers and Perry [29]. This solution generalizes the Reissner-Nordström solution [30] and it is given by

$$ds^2 = f(r)dt^2 - f(r)^{-1}dr^2 + r^2 d\Omega_{n+1}^2, \quad (1)$$

where

$$f(r) = 1 - \frac{C}{r^n} + \frac{D^2}{r^{2n}}, \quad (2)$$

with the constants related to the black hole mass M and charge Q by [29]

$$C = \frac{16\pi GM}{(n+1)\Omega_{n+1}}, \quad (3)$$

and

$$D = \pm \left(\frac{8\pi G}{n(n+1)} \right)^{1/2} Q. \quad (4)$$

Above, $d\Omega_{n+1}^2$ is the line element of a unit $(n+1)$ -sphere and

$$\Omega_{n+1} = \frac{2\pi^{\frac{n+2}{2}}}{\Gamma\left(\frac{n+2}{2}\right)}$$

is its area.

The spacetime given by Eq. (1) describes a black hole if $D^* \equiv 2|D|/C \leq 1$ and a naked singularity if $2|D|/C > 1$. In the first case, $f(r)$ possesses event horizons located at

$$r_{\pm} = \left(C/2 \pm \sqrt{C^2/4 - D^2} \right)^{1/n}. \quad (5)$$

Schwarzschild-Tangherlini black holes are obtained by letting $D \rightarrow 0$, in which case $r_- \rightarrow 0$. In the limit $|D| \rightarrow C/2$ we have an extreme black hole. In this case $r_- \rightarrow r_+$ and we have only one horizon.

Here we study small charged black holes on the 3-brane described by the ADD model [10]. In regions where $r \ll L$, where L is the size of the extra dimensions, Standard-Model particles will be subjected to the following geometry [18, 25]:

$$ds^2 = f(r)dt^2 - f(r)^{-1}dr^2 - r^2d\Omega_2^2, \quad (6)$$

with $f(r)$ given by Eq. (2), where $d\Omega_2^2$ represents the line element of a 2-sphere of unitary radius.

The dynamics of the massless scalar field is governed by the Klein-Gordon equation:

$$\frac{1}{\sqrt{-g}}\partial_{\mu}\left(\sqrt{-g}g^{\mu\nu}\partial_{\nu}\Phi\right) = 0, \quad (7)$$

where the metric $g^{\mu\nu}$ is given implicitly in Eq. (6), and g is its determinant.

A complete understanding of the scattering properties of a system requires the dynamic equations to be fully solved. However, the scattering problems of only a few systems have complete analytic solutions and one usually has to apply approximated and/or numeric methods [31]. The situation is similar in the context of black hole scattering [32]. In such cases, the main line adopted to solve the problem consists in separating the wave in partial waves with different angular momenta. Using the so-called ‘‘partial-wave method’’ requires a separation of variables. In the present case, we use the spherical symmetry of the spacetime to expand Φ in terms of partial waves proportional to the scalar spherical harmonics $Y_l^m(\theta, \phi)$, i.e., $\Phi_{\omega lm} = [\psi_{\omega l}(r)/r]Y_l^m(\theta, \phi)e^{-i\omega t}$. By doing so, the radial function $\psi_{\omega l}$ can be shown to satisfy the following equation:

$$f\frac{d}{dr}\left(f\frac{d\psi_{\omega l}}{dr}\right) + [\omega^2 - V_l(r)]\psi_{\omega l} = 0, \quad (8)$$

where the effective potential is given by

$$V_l(r) = f\left[\frac{f'}{r} + \frac{l(l+1)}{r^2}\right], \quad (9)$$

with the prime standing for differentiation with respect to r .

The effective potential tends to zero in two regions: (I) near the black hole horizon and (II) at infinity. Therefore, we can obtain approximated solutions for $\psi_{\omega l}$ in such regions. In order to do so, we introduce the tortoise coordinate defined as

$$\frac{d}{dr_*} = f\frac{d}{dr}, \quad (10)$$

so that the radial equation can be written as

$$\frac{d^2\psi_{\omega l}}{dr_*^2} + [\omega^2 - V_l(r_*)]\psi_{\omega l} = 0, \quad (11)$$

from where we can directly see that, for the scattering problem

$$\psi_{\omega l} \sim \begin{cases} A_{\omega l}^{\text{tr}}e^{-i\omega r_*} & \text{(region I);} \\ A_{\omega l}^{\text{in}}e^{-i\omega r_*} + A_{\omega l}^{\text{ref}}e^{i\omega r_*} & \text{(region II).} \end{cases} \quad (12)$$

The coefficients $A_{\omega l}^{\text{in}}, A_{\omega l}^{\text{ref}}, A_{\omega l}^{\text{tr}}$ are related to the incident, reflected and absorbed quantities of each partial wave. Here we consider a planar monochromatic wave impinging upon the black hole. By considering the initial wave as $\Phi_{\text{inc}} \propto e^{-i\omega z}$ we automatically remove the ϕ -dependence of the wave, once it is spinless. With such considerations, the scattering amplitude can be given in terms of partial waves by [32]:

$$f_{\omega}(\theta) = \frac{1}{2i\omega} \sum_{l=0}^{\infty} (2l+1) \left[e^{2i\delta_l(\omega)} - 1 \right] P_l(\cos \theta), \quad (13)$$

where $P_l(\cdot)$ are the Legendre polynomials and the phase shifts, $\delta_l(\omega)$, are defined by

$$e^{2i\delta_l(\omega)} = (-1)^{l+1} A_{\omega l}^{\text{ref}} / A_{\omega l}^{\text{in}}. \quad (14)$$

The differential scattering cross section follows directly from the scattering amplitude:

$$\frac{d\sigma_{\text{el}}}{d\Omega} = |f_{\omega}(\theta)|^2. \quad (15)$$

3 Approximations

Some approximations are useful to test the precision of our results. These are the case of the geodesic limit and the glory approximation. Other approximations can be used together with the numerical computation to improve the precision of our results in certain limits. This is the case of the Born approximation. We present such approximation methods below and compare them with the partial-wave-method results in Sec. 4.

3.1 High frequency

At high frequencies we can use the geodesic approach to describe the cross sections. Since we are working with massless particles, we have to consider null geodesics. From Eq. (6) we obtain:

$$\dot{s}^2 = f(r)\dot{t}^2 - f(r)^{-1}\dot{r}^2 - r^2(\dot{\theta}^2 + \sin^2 \theta \dot{\phi}^2) = 0, \quad (16)$$

where the dot denotes differentiation with respect to an affine parameter. Once again we can use the spherical symmetry of the problem to eliminate the θ -dependence of the motion by making $\theta = \pi/2$. Also, because of the symmetries of the spacetime, we have two motion constants

$$E = f\dot{t}, \quad (17)$$

and

$$L = r^2\dot{\phi}, \quad (18)$$

which are related to the energy and the angular momentum of the particle, respectively. Through these constants we can define the impact parameter as $b = L/E$. By doing so, after some manipulation, Eq. (16) results in

$$\left(\frac{du}{d\phi} \right)^2 = h_b(u) \equiv \frac{1}{b^2} - u^2 f(1/u), \quad (19)$$

where we have made the change of variable $r \rightarrow u = 1/r$. We can also take the derivative of (19) to generate a second-order differential equation for u . This leads to

$$\frac{d^2 u}{d\phi^2} + u = \left(\frac{n}{2} + 1 \right) C u^{n+1} - (n+1) D^2 u^{2n+1}. \quad (20)$$

By doing $d^2u/d\phi^2 = 0$ we can obtain the radius of the unstable orbit of the black hole for massless particles, $r_c = 1/u_c$. Substituting this value in $h_b(u)$ at Eq. (19) and equaling it to zero, we obtain the critical parameter $b_c = r_c/[f(r_c)]^{1/2}$. Particles which start their motion at infinity with $b < b_c$ will be absorbed by the black hole, while the ones with $b > b_c$ will be scattered back to infinity.

If we choose $b > b_c$, the smallest real root of $h_b(u)$ will describe the returning point of the geodesic, $u_0 = 1/r_0$. We are interested in computing the deflection angle $\Theta(b)$ which from (19) can be given by:

$$\Theta(b) = 2 \int_0^{u_0} h_b(u)^{-1/2} du - \pi. \quad (21)$$

The integration in Eq. (21) has known solutions in some cases, as in the case of 4-dimensional Schwarzschild ($n = 1$, $D = 0$) [33], Reissner-Nordström ($n = 1$, $|D| > 0$) [34], and the canonical acoustic black hole ($n = 4$, $D = 0$) [35]¹ generally written in terms of elliptic integrals. However, we cannot find a general expression for Eq. (21) here. Instead, we deal with it numerically in order to obtain results for the classical scattering cross section.

The scattering angle relates to the deflection angle as $\theta = |2m\pi - \Theta|$, where m are the number of times the geodesic circles the black hole. The classical scattering cross section can be given by

$$\frac{d\sigma_{\text{el}}^{(\text{cl})}}{d\Omega} = \sum_b \frac{b}{\sin \theta} \left| \frac{db}{d\theta} \right|, \quad (22)$$

where the sum in b takes into account the cases in which rays incoming with different bs are scattered in the same direction, i.e., same scattering angle but different deflections.

In Fig. 1 we present some results for the classical scattering cross section, Eq. (22). We have considered the cases $n = 2, 3$ with $D^* = 0, 0.7, 1$. For fixed values of n we see that the results are different in the near-backward direction but tend to be equal in the forward direction. This is an evidence that the charge plays a less important role as far from the black hole the particle passes. Also, the black holes scatters more as more charged they are since the differential scattering cross section is larger for higher values of D^* . Analogous results have been observed for other values of n and also in the case of Bardeen black holes [37].

3.2 Glory approximation

Geodesic approximation usually applies well in the limit of small scattering angles. Another approximation which can be useful to compare with the partial-wave results is the *glory* approximation [38, 32] valid in the limit $\theta \approx 180^\circ$. For spherically symmetric spacetimes, this approximation is given by the general formula:

$$\frac{d\sigma_{\text{el}}^{(\text{gl})}}{d\Omega} = 2\pi\omega b_g^2 \left| \frac{db}{d\theta} \right|_{\theta=\pi} J_{2s}^2(b_g\omega \sin \theta), \quad (23)$$

where b_g is the impact parameter of rays which are scattered at $\theta = 180^\circ$, s is the particle spin, and $J_\nu(\cdot)$ is the Bessel function of the first kind.

The values of $b_g^2|db/d\theta|_{\theta=\pi}$ and b_g will govern the intensity and the fringe widths which describe the interference pattern caused by rays scattered in opposite senses. These values vary according to the spacetime curvature, what makes

¹The effective metric which describes the canonical acoustic hole [36] is the same as the one of 7-dimensional Schwarzschild black holes induced on the 3-brane. However, the physics of the two systems is intrinsically different; the metric of the canonical acoustic hole is “seem” only by acoustic perturbations in the fluid flow which forms the hole [8].

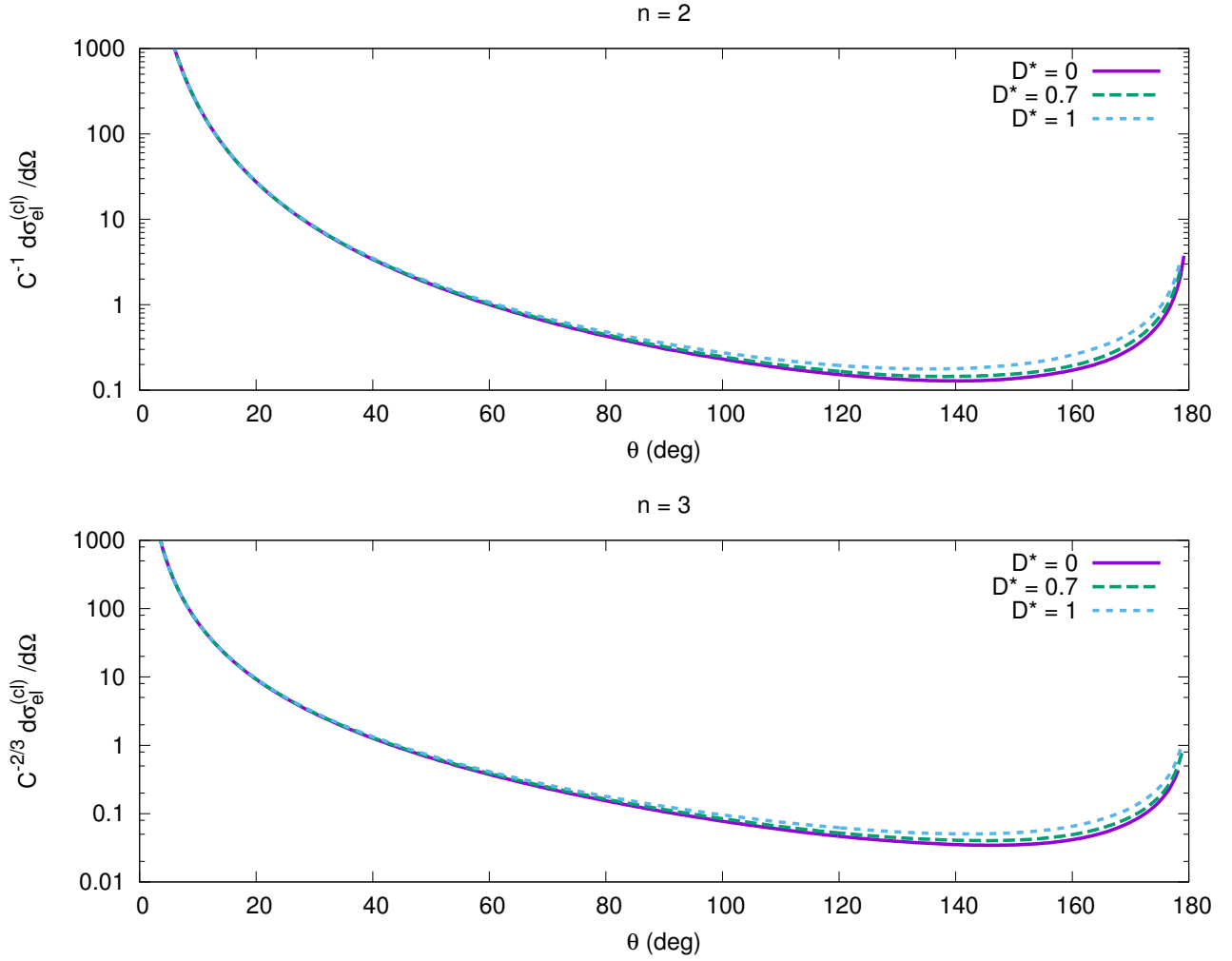


Figure 1: Null-geodesic scattering cross section localized on the 3-brane of higher-dimensional charged black holes. Here we have results for the cases $n = 2$ (top) and $n = 3$ (bottom).

each spacetime be identified by a different oscillatory pattern. The glory approximation (23) applies only if the scattered particle interferes with other particles without having its state altered. This is the case of most scattering processes around black holes, but it has a few exceptions, e.g., when helicity-reversing scattering takes place leading to non-zero backscattered electromagnetic radiation in Reissner-Nordström spacetimes [39].

Since we cannot find a general form for the deflection angle for all n and D^* , here we make numerical estimations for the cases which we compare with the results obtained via the partial-wave method in Sec. 4. Such estimations are listed in Tab. 1. From this table we can infer that b_g tends to decrease with the increase of D^* , while $|db/d\theta|$ tends to increase. Therefore, we can predict already that the fringes of interference will be wider as D^* increases for fixed n s or when n increases keeping the value of D^* unaltered. We cannot say much about the intensity of the peaks, since it is proportional to $b_g^2|db/d\theta|$. It has been shown in Ref. [34] that the glory intensity does not obey a monotonic behavior for the case $n = 1$, decreasing as the black hole charge intensity increases at first, but increasing again as $D^* \rightarrow 1$.

$n = 2$			
D^*	0	0.7	1
$C^{-1/2}b_g$	2.01	1.94	1.86
$C^{-1/2} db/d\theta $	1.29×10^{-2}	1.56×10^{-2}	2.16×10^{-2}
$n = 3$			
D^*	0	0.7	1
$C^{-1/3}b_g$	1.75	1.72	1.68
$C^{-1/3} db/d\theta $	3.48×10^{-3}	4.27×10^{-3}	5.90×10^{-3}
$n = 4$			
D^*	0	0.7	1
$C^{-1/4}b_g$	1.61	1.59	1.57
$C^{-1/4} db/d\theta $	1.22×10^{-3}	1.50×10^{-3}	2.03×10^{-3}

Table 1: Glory parameters for $n = 2$ (top), $n = 3$ (middle), and $n = 4$ (bottom) considering the cases $D^* = 0, 0.7, 1$.

3.3 Born approximation

Via the Born approximation [31], it can be shown that in the weak-field limit [24]:

$$\delta_l \approx \frac{\sqrt{\pi}}{2(n-1)} \frac{\Gamma\left(\frac{n+3}{2}\right)}{\Gamma\left(\frac{n+2}{2}\right)} \frac{\omega^n C}{(l+1/2)^{n-1}}. \quad (n > 1). \quad (24)$$

Although the formula above was obtained considering Schwarzschild black holes, it can be applied for charged black holes as well. This is justified by the fact that the Born approximation applied in the scattering from black holes is usually valid in the weak-field limit. However, in such limit, the most relevant term in the interaction between the black hole and uncharged particles comes from the mass term of the black hole, leading its charge to be important only in a second order. This is already clear in the 4-dimensional case, where the first order of the deflection angle in the weak-field regime depends only on the black hole mass, with the charge appearing only in the second-order term [40–42].

In order to make such analysis more quantitative, in Fig. 2 we compare the phase shifts obtained numerically in the case of extremely charged black holes for $n = 2$, $\omega C^{1/2} = 2.0$ and the Born approximation, Eq. (24). It is visible that these results agree very well already for $l \sim 20$. For larger values of n the spacetime becomes asymptotically flat even faster. Therefore, we expect that the agreement between the numerical phase shifts and the Born approximation to be very good for smaller values of l .

4 Results

In this section we present the results for the cross section obtained numerically via the partial-wave method. The method consists basically in computing the phase shifts (14) by comparing the numerical solution of the radial equation (8) with the asymptotic solutions (12). The sum in the scattering amplitude, Eq. (13), is developed through two different approaches, depending on the value of n . For $n \leq 3$, we use the phase shifts obtained numerically together with a method of reduced series described in Ref. [43] since the scattering amplitude sum converges purely in such cases. Therefore,

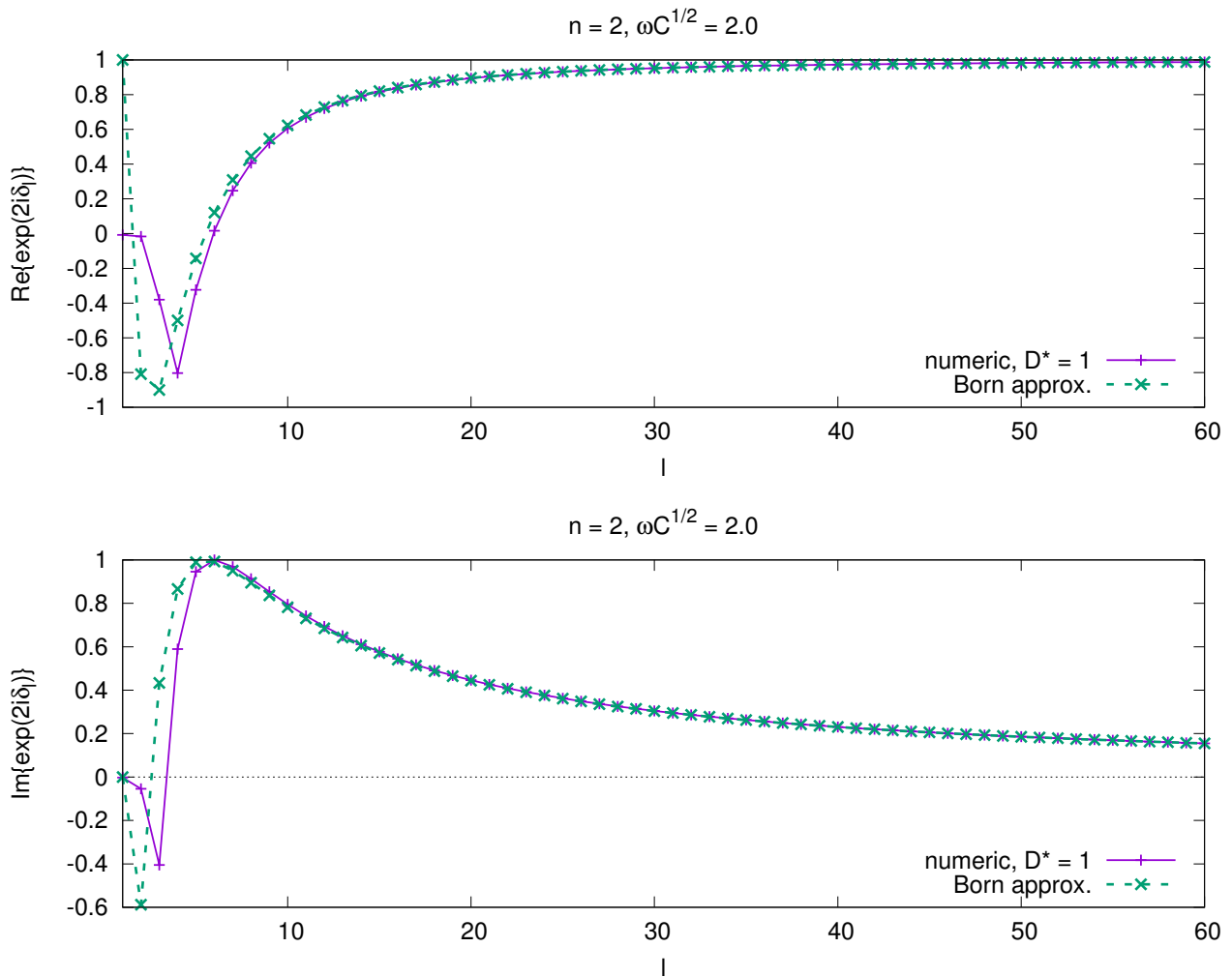


Figure 2: Comparison of phase shifts obtained numerically ($D^* = 1$) and via Born approximation, Eq. (24), for $n = 2$ and $\omega C^{1/2} = 2.0$.

this method guarantees that we will obtain convergent scattering amplitudes considering a relative small number of phase shifts [44]. For $n > 3$, the cases in which the differential scattering cross section is finite in the entire range of θ [24], we split the scattering amplitude in two. The first part is computed with the sum of terms which include phase shifts obtained numerically until l_m . The rest of the series is then computed with the phase shifts obtained via Born approximation, Eq. (24), from $l_m + 1$ until l_{\max} , with l_m within the regime of validity of Eq. (24). This approach has been introduced to the study of black hole scattering in Ref. [35].

In Fig. 3 we present the scalar differential scattering cross sections for charged black holes on the brane for $n = 1, 2, 3, 4$, $D^* = 0, 0.7, 1$, and $\omega C^{1/n} = 2.0$. As we can see, the charge of the black hole plays an important role in the scattering for large values of θ . In this regime, the widths of interference tend to wider with the increase of D^* , as anticipated in Tab. 1, where we observed that b_θ decreases with the increase of D^* . We observe an increase in the intensity of the interference peaks in the cases $n > 1$, but not in the case $n = 1$, as already observed in Ref. [34]. For low values of θ the charge of the black hole has little influence in the scattering, and we can observe that the results for $D^* = 0, 0.7, 1$ for all values of n presented tend to coincide in the regime $\theta \lesssim 40^\circ$.

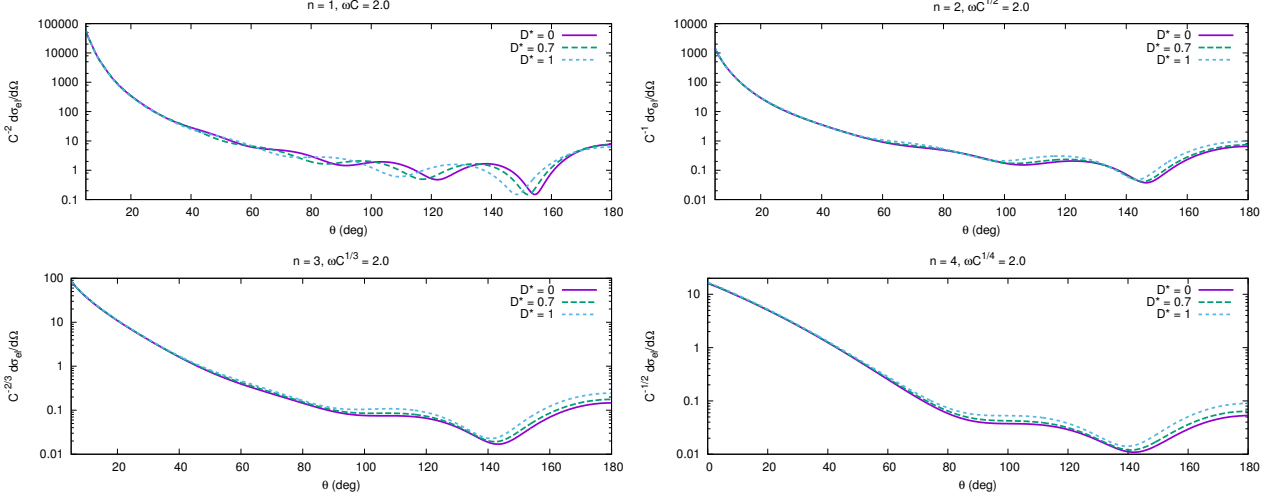


Figure 3: Scattering cross section of charged black holes for the massless scalar field on the 3-brane for $n = 1$ (top-left), $n = 2$ (top-right), $n = 3$ (bottom-left), and $n = 4$ (bottom-right).

We compare the numerical results with the geodesic and glory approximations, presented in Secs. 3.1 and 3.2 respectively, in Fig. 4. There we consider a relative high value of frequency ($\omega C^{1/n} = 10.0$) once such approximations are valid in the high-frequency regime. We see that the agreement with the glory approximation is excellent in all cases for $\theta \gtrsim 160^\circ$. The geodesic approximation, however, is only a very good approximation in the cases $n = 1, 2, 3$, but not in the case $n = 4$. In this case the geodesic method predicts that the flux scattered in the forward direction should be infinity while the wave analysis predicts a finite flux in the same direction. We expect the geodesic approximation being recovered only in the classical limit, i.e., $\omega C^{1/n} \rightarrow \infty$, for the cases in which $n \geq 4$. Although we presented only results for extreme black holes in Fig. 4, we have observed similar agreements for the cases $D^* < 1$. The same comparison has been done for the case of uncharged black holes in Ref. [24] with similar conclusions.

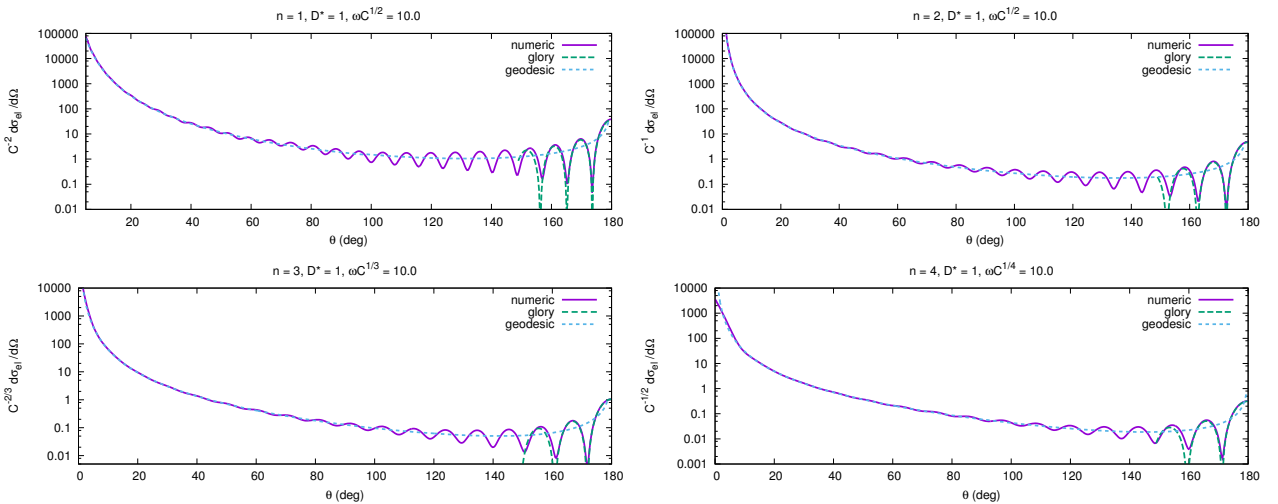


Figure 4: Comparisons of the differential scattering cross section obtained via the partial-wave method and via the geodesic and glory approximations. Here we consider extremal black holes in all cases with $\omega C^{1/n} = 10.0$.

Figure 5 shows a comparison of the scattering cross sections for extremely charged black holes in spacetimes with different dimensions, namely $n = 1, 2, 3, 4$ (case $n = 1$ has been extensively studied in Ref. [34]). Similarly to what happens with uncharged black holes [24], the increase in the number of dimensions implies in weaker interactions between the black hole and the test field. As a consequence, the intensity of scattered flux by the black hole decreases as n increases. The fringes of interference get wider with the increase of n . This is in agreement with the results presented in Tab. 1, where we observed a decrease of b_g with the increase of n .

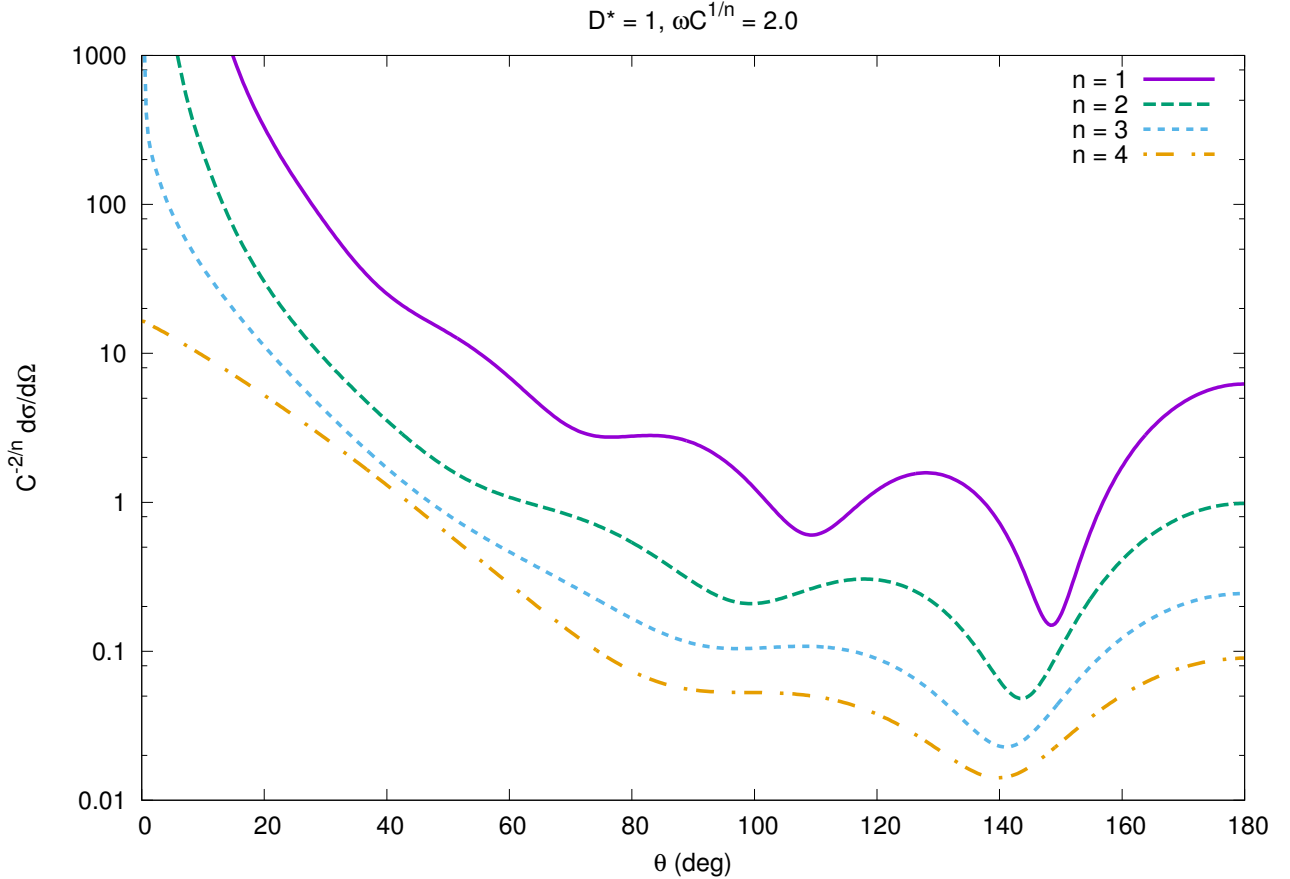


Figure 5: Comparison of the scattering cross sections for extremely charged black holes in spacetimes with different number of dimensions. Here we consider $\omega C^{1/n} = 2.0$.

5 Final remarks

We have computed the differential scattering cross section for the massless scalar field localized on the 3-brane of higher-dimensional charged black holes in the ADD model. We have focused mainly in the case of extremal black holes, but also presented results for non-extremal and uncharged black holes. The latter case has been extensively studied in Ref. [24]. Although we showed results only for the cases $n = 1, 2, 3, 4$ our analysis could be straightforwardly generalized for higher values of n .

We would like to remark the fact that there is an important transition in the behavior of the cross section when changing

the spacetime dimensionality from $n < 4$ to $n \geq 4$. For the cases $n \geq 4$, the differential scattering cross section is finite in all directions, while it diverges in the forward direction for the cases $n < 4$. This has been foreseen based in the Born approximation in Ref. [24] for uncharged black holes, but the conclusions there can be applied equally to the cases studied here since the effects of the black hole charge can be neglected in the weak-field limit. This has been evidenced in the results obtained via geodesic (Fig. 1) and partial-wave (Fig. 3) methods where we have observed that the curves which describe the differential scattering cross sections for different charges tend to approach each other with the decrease of θ , being almost indistinguishable at $\theta \lesssim 40^\circ$.

The results obtained via partial-wave method were compared with two approximations: (i) the geodesic approximation and (ii) the glory approximation. Both comparisons resulted in excellent agreements in their regime of validity for the cases $n \leq 3$; small angles in case (i) and large angles in case (ii). For $n = 4$, the agreement is excellent in case (ii) but not in case (i) since the classical approximation predicts a divergence in the differential scattering cross section in the limit $\theta \rightarrow 0$, while the wave analysis reveals that the scattered flux is actually finite in such limit. The same disagreement between the partial-wave method and the geodesic approximation is expected to happen in the cases $n > 4$, unless one considers $\omega C^{1/n} \rightarrow \infty$.

Acknowledgments

The author would like to thank to Conselho Nacional de Desenvolvimento Científico e Tecnológico (CNPq) and Coordenação de Aperfeiçoamento de Pessoal de Nível Superior (CAPES) for partial financial support.

References

- [1] B. P. Abbott et al. Observation of Gravitational Waves from a Binary Black Hole Merger. *Phys. Rev. Lett.*, 116(6): 061102, 2016. doi: 10.1103/PhysRevLett.116.061102.
B. P. Abbott et al. GW151226: Observation of Gravitational Waves from a 22-Solar-Mass Binary Black Hole Coalescence. *Phys. Rev. Lett.*, 116(24):241103, 2016. doi: 10.1103/PhysRevLett.116.241103.
B. P. Abbott et al. GW170104: Observation of a 50-Solar-Mass Binary Black Hole Coalescence at Redshift 0.2. *Phys. Rev. Lett.*, 118(22):221101, 2017. doi: 10.1103/PhysRevLett.118.221101.
- [2] M. C. Begelman. Evidence for black holes. *Science*, 300:1898–1903, 2003. doi: 10.1126/science.1085334.
- [3] Tim Johannsen. Sgr A* and General Relativity. *Class. Quant. Grav.*, 33(11):113001, 2016. doi: 10.1088/0264-9381/33/11/113001.
- [4] Tim Johannsen, Avery E. Broderick, Philipp M. Plewa, Sotiris Chatzopoulos, Sheperd S. Doeleman, Frank Eisenhauer, Vincent L. Fish, Reinhard Genzel, Ortwin Gerhard, and Michael D. Johnson. Testing General Relativity with the Shadow Size of Sgr A*. *Phys. Rev. Lett.*, 116(3):031101, 2016. doi: 10.1103/PhysRevLett.116.031101.
- [5] Scott C. Noble, Po Kin Leung, Charles F. Gammie, and Laura G. Book. Simulating the emission and outflows from accretion discs. *Class. Quant. Grav.*, 24:S259–S274, 2007. doi: 10.1088/0264-9381/24/12/S17.

- [6] Andy Bohn, William Thrope, Fran Hébert, Katherine Henriksson, Darius Bunandar, Mark A. Scheel, and Nicholas W. Taylor. What does a binary black hole merger look like? *Class. Quant. Grav.*, 32(6):065002, 2015. doi: 10.1088/0264-9381/32/6/065002.
- [7] Heino Falcke, Fulvio Melia, and Eric Agol. Viewing the Shadow of the Black Hole at the Galactic Center. *Astrophys. J.*, 528:L13, 2000. doi: 10.1086/312423.
- [8] W. G. Unruh. Experimental Black-Hole Evaporation? *Phys. Rev. Lett.*, 46:1351–1353, 1981. doi: 10.1103/PhysRevLett.46.1351.
- [9] Carlos Barceló, Stefano Liberati, and Matt Visser. Analogue Gravity. *Living Rev. Rel.*, 8:12, 2005. doi: 10.12942/lrr-2005-12. [Living Rev. Rel.14,3(2011)].
- [10] Nima Arkani-Hamed, Savas Dimopoulos, and Gia R. Dvali. The hierarchy problem and new dimensions at a millimeter. *Phys. Lett. B*, 429:263–272, 1998. doi: 10.1016/S0370-2693(98)00466-3.
Ignatios Antoniadis, Nima Arkani-Hamed, Savas Dimopoulos, and Gia Dvali. New dimensions at a millimeter to a fermi and superstrings at a tev. *Physics Lett. B*, 436:257–263, 1998.
- [11] Lisa Randall and Raman Sundrum. A Large mass hierarchy from a small extra dimension. *Phys. Rev. Lett.*, 83: 3370–3373, 1999. doi: 10.1103/PhysRevLett.83.3370.
- [12] Marco Cavaglia. Black hole and brane production in TeV gravity: A Review. *Int. J. Mod. Phys. A*, 18:1843–1882, 2003. doi: 10.1142/S0217751X03013569.
- [13] Panagiota Kanti. Black holes in theories with large extra dimensions: A Review. *Int. J. Mod. Phys. A*, 19:4899–4951, 2004. doi: 10.1142/S0217751X04018324.
- [14] Roberto Emparan and Harvey S. Reall. Black Holes in Higher Dimensions. *Living Rev. Rel.*, 11:6, 2008. doi: 10.12942/lrr-2008-6.
- [15] S. W. Hawking. Particle creation by black holes. *Commun. Math. Phys.*, 43:199–220, 1975. doi: 10.1007/BF02345020. [,167(1975)].
- [16] Silke Weinfurter, Edmund W. Tedford, Matthew C. J. Penrice, William G. Unruh, and Gregory A. Lawrence. Measurement of Stimulated Hawking Emission in an Analogue System. *Phys. Rev. Lett.*, 106:021302, 2011. doi: 10.1103/PhysRevLett.106.021302.
- [17] Theo Torres, Sam Patrick, Antonin Coutant, Mauricio Richartz, Edmund W. Tedford, and Silke Weinfurter. Observation of superradiance in a vortex flow. 2016.
- [18] Roberto Emparan, Gary T. Horowitz, and Robert C. Myers. Black Holes Radiate Mainly on the Brane. *Phys. Rev. Lett.*, 85:499–502, 2000. doi: 10.1103/PhysRevLett.85.499.
- [19] Panagiota Kanti and John March-Russell. Calculable corrections to brane black hole decay: The scalar case. *Phys. Rev. D*, 66:024023, 2002. doi: 10.1103/PhysRevD.66.024023.

- [20] Panagiota Kanti and John March-Russell. Calculable corrections to brane black hole decay. II. Greybody factors for spin 1/2 and 1. *Phys. Rev. D*, 67:104019, 2003. doi: 10.1103/PhysRevD.67.104019.
- [21] Chris M. Harris and Panagiota Kanti. Hawking radiation from a $(4 + n)$ -dimensional black hole: exact results for the Schwarzschild phase. *JHEP*, 10:014, 2003. doi: 10.1088/1126-6708/2003/10/014.
- [22] Eylee Jung, SungHoon Kim, and D. K. Park. Low-energy absorption cross section for massive scalar and Dirac fermion by $(4+n)$ -dimensional Schwarzschild black hole. *JHEP*, 09:005, 2004. doi: 10.1088/1126-6708/2004/09/005.
- [23] P. Kanti, Julien Grain, and A. Barrau. Bulk and brane decay of a $(4 + n)$ -dimensional Schwarzschild–de Sitter black hole: Scalar radiation. 71:104002, 2005. doi: 10.1103/PhysRevD.71.104002.
- [24] Cássio I. S. Marinho and Ednilton S. de Oliveira. Scattering of massless scalar waves from Schwarzschild-Tangherlini black holes on the brane. *arXiv*, page 1612.05604, 2016.
- [25] Eylee Jung and D. K. Park. Absorption and emission spectra of an higher-dimensional Reissner-Nordström black hole. *Nucl. Phys. B*, 717:272–303, 2005. doi: 10.1016/j.nuclphysb.2005.03.037.
- [26] S. Creek, O. Efthimiou, P. Kanti, and K. Tamvakis. Greybody factors for brane scalar fields in a rotating black hole background. *Phys. Rev. D*, 75:084043, 2007. doi: 10.1103/PhysRevD.75.084043.
- [27] Bobir Toshmatov, Zdeněk Stuchlík, Jan Schee, and Bobomurat Ahmedov. Quasinormal frequencies of black hole in the braneworld. *Phys. Rev. D*, 93(12):124017, 2016. doi: 10.1103/PhysRevD.93.124017.
- [28] C. Molina, A. B. Pavan, and T. E. Medina Torrejón. Electromagnetic perturbations in new brane world scenarios. *Phys. Rev. D*, 93(12):124068, 2016. doi: 10.1103/PhysRevD.93.124068.
- [29] Robert C. Myers and M. J. Perry. Black holes in higher dimensional space-times. *Annals Phys.*, 172:304, 1986. doi: 10.1016/0003-4916(86)90186-7.
- [30] Subrahmanyan Chandrasekhar. *The Mathematical Theory of Black Holes*. Clarendon Press, Oxford, 1983. ISBN 0-19-851291-0.
- [31] Kurt Gottfried and Tung-Mow Yan. *Quantum Mechanics: Fundamentals*. Springer, New York, 2 edition, 2004. ISBN 0-387-22823-2.
- [32] J. A. H. Futterman, F. A. Handler, and R. A. Matzner. *Scattering from Black Holes*. Cambridge University Press, Cambridge, 1988. ISBN 0-521-32986-8.
- [33] Charles Darwin. The gravity field of a particle. *Proceedings of the Royal Society of London A: Mathematical, Physical and Engineering Sciences*, 249(1257):180–194, 1959. ISSN 0080-4630. doi: 10.1098/rspa.1959.0015. URL <http://rspa.royalsocietypublishing.org/content/249/1257/180>.
- [34] Luis C. B. Crispino, Sam R. Dolan, and Ednilton S. Oliveira. Scattering of massless scalar waves by Reissner-Nordstrom black holes. *Phys. Rev. D*, 79:064022, 2009. doi: 10.1103/PhysRevD.79.064022.

- [35] Sam R. Dolan, Ednilton S. Oliveira, and Luis C. B. Crispino. Scattering of sound waves by a canonical acoustic hole. *Phys. Rev. D*, 79:064014, 2009. doi: 10.1103/PhysRevD.79.064014.
- [36] Matt Visser. Acoustic black holes: horizons, ergospheres and Hawking radiation. *Class. Quant. Grav.*, 15:1767–1791, 1998. doi: 10.1088/0264-9381/15/6/024.
- [37] Caio F. B. Macedo, Ednilton S. de Oliveira, and Luís C. B. Crispino. Scattering by regular black holes: Planar massless scalar waves impinging upon a Bardeen black hole. *Phys. Rev. D*, 92(2):024012, 2015. doi: 10.1103/PhysRevD.92.024012.
- [38] Richard A. Matzner, Cécile DeWitte-Morette, Bruce Nelson, and Tian-Rong Zhang. Glory scattering by black holes. *Phys. Rev. D*, 31(8):1869, 1985. doi: 10.1103/PhysRevD.31.1869.
- [39] Luís C. B. Crispino, Sam R. Dolan, Atsushi Higuchi, and Ednilton S. de Oliveira. Inferring black hole charge from backscattered electromagnetic radiation. *Phys. Rev. D*, 90(6):064027, 2014. doi: 10.1103/PhysRevD.90.064027.
- [40] Ernesto F. Eiroa, Gustavo E. Romero, and Diego F. Torres. Reissner-Nordström black hole lensing. *Phys. Rev. D*, 66:024010, 2002. doi: 10.1103/PhysRevD.66.024010.
- [41] A. Bhadra. Gravitational lensing by a charged black hole of string theory. *Phys. Rev. D*, 67:103009, 2003. doi: 10.1103/PhysRevD.67.103009.
- [42] Mauro Sereno. Weak field limit of Reissner-Nordström black hole lensing. *Phys. Rev. D*, 69:023002, 2004. doi: 10.1103/PhysRevD.69.023002.
- [43] D. R. Yennie, D. G. Ravenhall, and R. N. Wilson. Phase-Shift Calculation of High-Energy Electron Scattering. *Phys. Rev.*, 95:500–512, 1954. doi: 10.1103/PhysRev.95.500.
- [44] Sam Dolan, Chris Doran, and Anthony Lasenby. Fermion scattering by a Schwarzschild black hole. *Phys. Rev. D*, 74:064005, 2006. doi: 10.1103/PhysRevD.74.064005.